Fire design of post-installed bonded rebars: Full-scale validation test on a 2.94 x 2 x 0.15 m 3 concrete slab subjected to ISO 834-1 fire

Mohamed Amine Lahouar, Nicolas Pinoteau, Jean-François Caron, Gilles Forêt, Philippe Rivillon

Final version of the paper published in Engineering Structures, 174, October 2018, p. 81-94 [https://doi.org/10.1016/j.engstruct.2018.07.069]

Fire design of post-installed bonded rebars: Full-scale validation test on a 2.94 x 2 x 0.15 m^3 concrete slab subjected to ISO 834-1 fire

Mohamed Amine Lahouar[a,b,*], Nicolas Pinoteau[b], Jean-François Caron[a], Gilles Foret[a], Philippe Rivillon[b]

[a] Université Paris-Est, Laboratoire Navier (UMR 8205), Ecole des Ponts ParisTech, F-77455 Marne-la-Vallée, France
[b] Université Paris-Est, Centre Scientifique et Technique du Bâtiment (CSTB), 84 avenue Jean Jaurès, Champs-sur-Marne, 77447 Marne-la-Vallée Cedex 2, FRANCE.

*__Corresponding author.__ Tel: +33630242016. E-mail address: amine.lahouar@enpc.fr. Present address: 6-8 Avenue Blaise Pascal, Ecole Nationale des Ponts et Chaussées, 77420 Champs-sur-Marne, France.

Abstract
Thanks to the improvement in mechanical and adhesion properties of polymer resins, Post-Installed Rebars (PIRs) succeeded progressively in replacing cast-in place rebars in some applications by offering equivalent or even higher mechanical properties at ambient temperature. However, the mechanical behavior of PIRs is essentially governed by the mechanical behavior of polymer resins, which is highly sensitive to temperature. Consequently, fire safety presents a potential hazard that should be taken into account when designing. This paper presents an experimental full-scale fire test carried out on the Vulcain furnace of CSTB Champs-sur-Marne on its 7m x 4 m horizontal configuration, in order to test a new fire design method proposed for PIRs. The 2.94 x 2 x 0.15 m^3 tested slab was mechanically loaded by 325 kg and heated following the ISO 834-1 time-temperature curve until its collapse. The experimental time of collapse is compared to that predicted by the new design method.

Keywords: Chemical post-installed rebars, Full-scale fire test, Cantilever slab-wall connection, Bond strength, Fire design method.

1. Introduction

Anchoring systems are used in reinforced concrete structures in order to ensure the stress transfer between two neighboring structural elements [1]. Their installation can be carried out using two different methods. The first method, called “Cast-in-place rebars”, consists in placing a steel rebar in a desired position in the formwork and then casting the concrete around. While, the second method, called “Post-installed rebars”, consists in embedding the steel rebar inside a hole drilled into the hardened concrete [2]. Post-installed rebars (PIRs) offer advantageous solutions for concrete construction by proposing a viable and economical method for adding new concrete sections or attaching steel members to existing structures [3] [4]. Indeed, PIRs were initially used for correcting fabrication errors in precast concrete, and then in retrofitting, extending and repairing existing structures [5] [6]. Today, PIRs are also used in new constructions to meet the high architectural requirements by providing more flexibility in the planning and design of concrete structures [7].

Post-installed bonded rebars can be divided into two groups according to the bonding agents used for the rebar setup [8]. “Chemical post-installed rebars”, where rebars are bonded using chemical bonding agents such as polyester, vinylester and epoxy resins, and “Grouted rebars”, where rebars are bonded using nonchemical bonding agents such as mortars and cement grout [3]. Mortars and cement grout can be easily pumped into deep embedded holes, which allows making PIRs with high load bearing capacity [9]. However grouted rebars require a long curing time and generally a large hole diameter. Nevertheless, chemical post-installed rebars provide a high load bearing capacity using small hole

diameter and embedment length. Therefore, the use of chemical PIRs in concrete constructions is today more suitable than grouted rebars. Indeed, the preference for chemical PIRs is the result of the minimization of the curing time of chemical bonding agents by the introduction of fast-curing adhesives, and is also the result of the high stiffness provided by the fillers added to structural resins in order to increase their viscosity and mechanical properties [10] [11].

Several experimental research studies have been conducted in order to compare the mechanical behavior between the various existing anchoring systems. *Spieth et al.* [12] had carried-out a series of pull-out tests on cast-in-place rebars, chemical PIRs bonded with epoxy and polyester resins and on hybrid PIRs bonded with a combination of vinylester and cementitious compounds. Results showed that the hybrid system had a mechanical behavior very close to cast-in-place rebars with a slightly better bond resistance. While chemical PIRs bonded with epoxy resin showed a much higher stiffness and a larger bond strength than cast-in-place rebars. However, chemical PIRs bonded with polyester resin showed a softer behavior and a significantly lower bond strength than all other systems. These results were subsequently confirmed by *Rosca et al.* [13] with an experimental study on grouted rebars bonded with a cement mortar. Results showed that the mechanical behavior of grouted rebars was very close to cast-in-place rebars. Thus, the comparison between the different anchoring systems showed that in general, PIRs bonded with epoxy resins provide higher mechanical properties than all other anchoring systems.

The mechanical behavior of chemical PIRs is governed by several parameters such as materials and geometric parameters [1] [14] [15] [11], the installation process [16] [17] [18] [19] and by the environmental factors to which they are subjected. Several studies had confirmed the sensitivity of polymer resins to environmental factors such as moisture and temperature [20] [21] [22]. Indeed, temperature seems to be the factor that affects the most the mechanical behavior of chemical PIRs. In a previous paper [23], we showed that the temperature increase up to values blow the resin glass transition temperature leads to increase the mechanical properties of chemical PIRs due to the resin post-cure phenomenon. However, when temperature exceeds the resin glass transition temperature, a change in viscosity and physical state occur [24], leading therefore to a new bond stress distribution along the bond joint [25] [26]. The influence of the heating increase rate was studies in [5], and it is shown that high heating rates can generate a thermal gradient along the steel rebar and consequently can lead to a new bond stress distribution. To conclude, the mechanical behavior of chemical PIRs at high temperature seems to be very complex due to several mechanical and physicochemical changes happening at the adhesive joint, affecting its mechanical properties [23] [27]. Therefore, fire is a potential hazard which should be taken into account when designing structures containing chemical PIRs [28].

Finally, several evaluation methods and design rules exist today in order to design and to secure the use of chemical PIRs at normal operating temperatures [29] [30] [31] [32] [33]. Nevertheless, few researchers have focused on the variation of the mechanical behavior of PIRs at high temperature and have suggested design methods in case of fire. *Zhang el al.* [22] has carried out several pull-out tests at different temperatures and proposed an empirical method allowing deducing the bond stress value at different temperature ranges. *Pinoteau et al.* [26], *Eligehausen et al.* [34] and *Lahouar et al.* [23] have proposed a "bond resistance integration method" allowing predicting the time of collapse of post-installed rebars using thermal calculations and bond resistance variation at different temperatures. This method was validated in [26] by performing a full-scale ISO fire test on a cantilever-wall connection using chemical PIRs and figures today on the European Assessment Document (EAD) 330087-00-06.01 [35].

This paper presents an experimental full-scale fire test on a cantilever concrete slab (2.94 m x 2 m x 0.15 m) connected to a wall using 8 chemical post-installed rebars. This paper aims to predict the time of collapse of PIRs under mechanical and thermal loading (according to the ISO 834-1 time-temperature curve [36]), in order to compare between experimental and calculated times of collapse.

The calculation method used to predict the fire resistance of post-installed rebars was inspired from that presented in the European Assessment Document (EAD) 330087-00-06.01 [35]. The goal was to verify the relevance of the proposed design method on a new configuration, other than that tested in [26]. The first part of this paper explains and details the design method used to predict the fire resistance of chemical post-installed rebars in a concrete structure, and then shows how it can be applied in the case of a slab-wall connection. The second part presents the full-scale fire test used to validate the design method. Analyses and discussion are developed in the last part to explain the phenomena that occurred and led to the collapse of the slab, and finally to conclude on the accuracy and the weakness of the method.

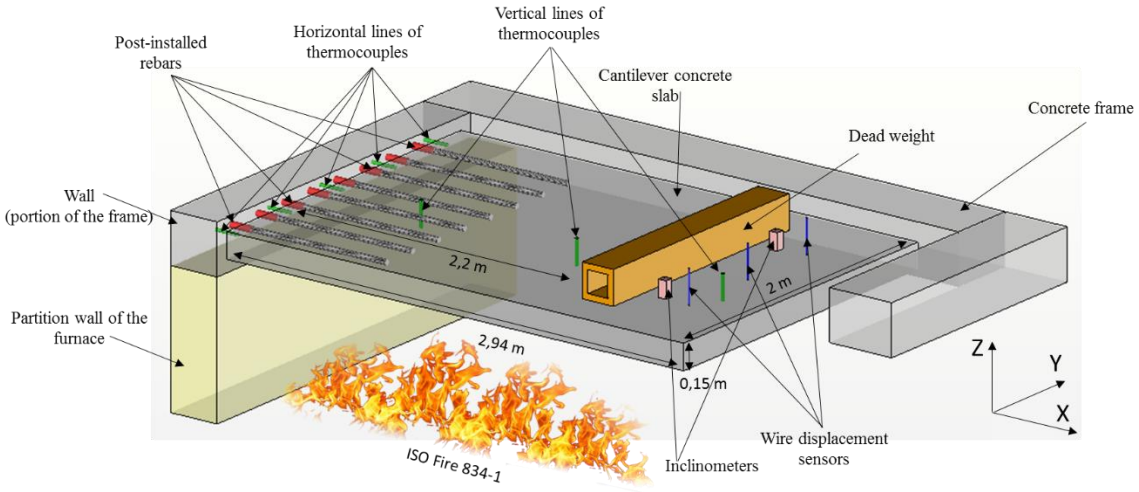

Fig 1: Vulcain fire test configuration: Instrumentation and set up on the furnace

2. Fire design method description

The bond resistance integration method is a design method allowing to calculate the evolution of the bearing capacity of a PIR subjected to a temperature variation and then to predict its time of collapse. To reach this goal, the design method requires the knowledge and the determination of several parameters. The prediction of the time of collapse of a structure containing PIRs requires five steps.

1- Determination of the applied load (F_{app})

PIRs embedded in concrete structures have the function of transferring the tensile forces applied on the concrete section. The first step in calculating the fire resistance of PIRs consists in determining the applied load, which can be done either by analytical calculations (Eurocode 2 part 1-1 method [29]) or by finite element analysis. In all cases, this step requires the knowledge of some parameters such as the geometric parameters of the structure, the concrete density and the position of the steel rebar in the structure...

2- Temperature mapping ($\theta(x,t)$)

After determining the amount of tensile load applied on the PIRs, the next step consists in determining the temperature distribution at each element of the bond and at different moments of fire exposure, using thermal calculations. Thermal calculations can be done either by finite element analysis, or using finite difference method to solve Fourier's equations (*Eq. (1), (2) and (3)*). Regardless of the chosen method, it is necessary to know the thermal properties of the PIR components (*thermal conductivity* $\lambda(\theta)$*, specific heat* $C_p(\theta)$ *and materials density* $\rho(\theta)$) to be able to perform thermal calculations. Materials thermal properties can be determined by carrying out appropriate tests or can be directly found in design guides such as Eurocode 2 part 1-2 [36].

$$\rho(\theta(x,t)).C_p(\theta(x,t)).\frac{\partial\theta(x,t)}{\partial t}=\lambda(\theta(x,t)).\frac{\partial^2\theta(x,t)}{\partial x^2} \quad (1)$$

$$\dot{q}_{conv}= h(\theta_{ext}(x,t)-\theta_{surf}(x,t)) \quad (2)$$

$$\dot{q}_{rad}= \sigma.\varepsilon.(\theta^4_{ext}(x,t)-\theta^4_{sur}(x,t)) \quad (3)$$

Where ρ is the material density [kg/m^3]
C_p is the material specific heat [J. K^{-1}. Kg^{-1}]
λ is the material thermal conductivity [W. m^{-1}. K^{-1}]
$\theta(x,t)$ is the temperature of an element of the PIR at position x and at time t [K]
$\dot{q}_{conv}$ is the convective heat flux [W. m^{-2}]
$\dot{q}_{rad}$ is the radiative heat flux [W. m^{-2}]
h is the heat transfer coefficient [W.m^{-2}.K^{-1}]
σ is the Stefan-Boltzmann constant [W.m^{-2}.K^{-4}]
ε is the emissivity of the material
θ_{ext} is the gas temperature [K]
θ_{sur} is the temperature at the surface of the material [K]

3- Bond strength –temperature relationship ($\tau_{max}(\theta)$)

The third step in the calculation of the evolution of the PIR bearing capacity is to assign a bond resistance value to each element of the PIR depending on its temperature. This step relies on the bond strength-temperature relationship obtained by pull-out tests at high temperature [5] [23] performed on chemical PIRs made from the same resin.

4- Calculation of the load baring capacity (F_t)

At the end of the previous step, a bond resistance distribution is obtained over the whole PIR embedment length for each moment of fire exposure. Thus, the load bearing capacity of the post-installed bonded rebar at a given moment "t" of the fire exposure can be obtained by integrating the bond resistances at the time "t" over the entire embedment length following *Eq. (4)*.

$$F_t=2.\pi.r\int_0^L \tau_{max}(\theta(x,t))\,dx \quad (4)$$

Where F_t is the load bearing capacity of the PIR at time t [N]
r is the radius of the steel rebar [mm]
L is the embedment length [mm]
τ_{max} is the bond resistance obtained by pull-out tests [MPa]
$\theta(x,t)$ is the temperature of an element of the PIR at position x and at time t [K].

5- Time of collapse

The design model assumes that failure occurs when the shear stress reaches the bond strength at all elements composing the PIR. Therefore, the time of collapse is considered as the time at which the load bearing capacity becomes equal to, or lower than the tensile load applied to the steel rebars, i.e. when $F_t \leq F_{app}$.

Fig. 2 summarizes the main steps of the calculation of the bearing capacity evolution of PIRs during a fire exposure using the bond resistance integration method, as represented by *Pinoteau et al.* [26].

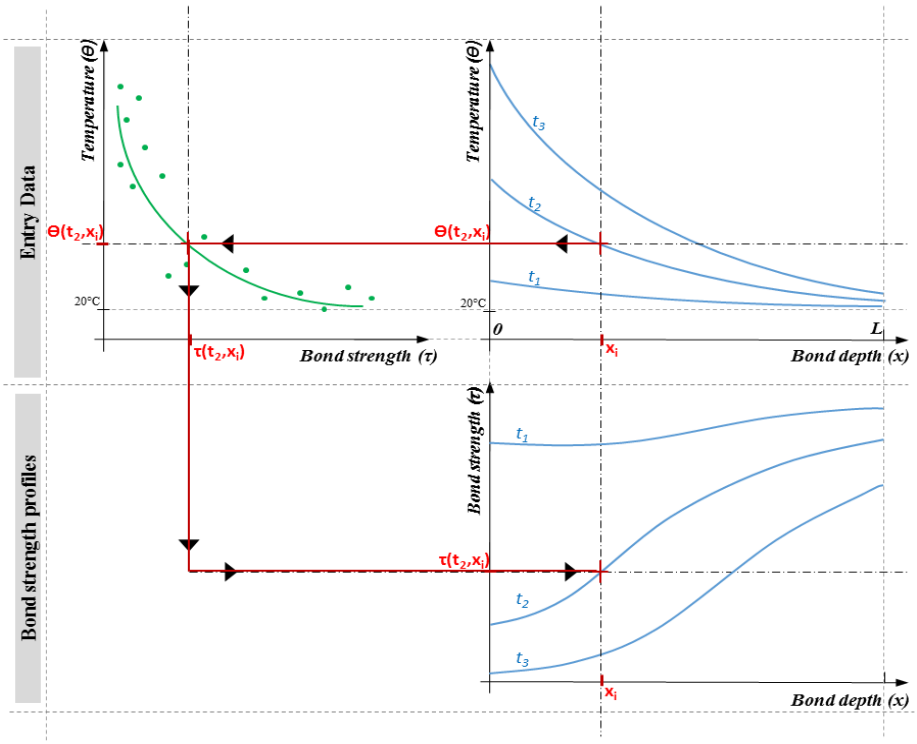

Fig. 2: Bond resistance integration design method applied to chemical PIRs subjected to fire (Pinoteau et al. [26])

3. Test Specimen set-up and design method application

3.1 Test specimen conception

The objective of this section is to explain how the configuration and the dimensions of the test specimen were chosen in order to evaluate the fire resistance of PIRs on a full-scale wall-slab connection.

The full-scale fire test was carried out on the "Vulcain" modular gas furnace of CSTB Champs-sur-Marne, France (Fig. 3). The furnace offers three possible exposure areas to perform fire tests in the horizontal configuration: 3m x 3m, 4m x 3m and 7m x 3m. The fire test presented in this paper was performed on the 4 m x 3 m horizontal configuration. The test specimen configuration was composed of a concrete slab attached to a wall by post-installed rebars. The choice of this configuration can be justified by the fact that it could be representative of balconies maintained by chemical PIRs sealed into a concrete wall. The set-up of the test specimen on the furnace required the presence of a concrete frame allowing to close the furnace and to ensure its fire integrity during the test. The concrete frame was made from a C45/55 reinforced concrete containing propylene fibers, and represents the wall in which post-installed rebars are anchored. The configuration and dimensions chosen for the test specimen were a 2.94 m x 2 m x 0.15 m cantilever slab made from C20/25 reinforced concrete containing propylene fibers, connected to the wall by means of 8 post-installed rebars, bonded into concrete using an epoxy resin (Fig. 1). The number of PIRs was determined according to the EC2 part 1-1 design rules [29] which allow a maximum spacing between bonded rebars equal to two times the thickness of the slab (i.e. 300 mm). The diameter of the steel rebars was chosen equal to 16 mm and the embedment length was set at 135 mm. The thickness of the bond joint was equal to 2 mm, according to the resin supplier's recommendations. A spacing of 80 mm at the sides and 200 mm at the free end of the cantilever slab was left to take into account the thermal expansion and the rotation of the slab, in order to prevent any possible blocking against the frame during the fire test (Fig. 4). The test specimen was mechanically loaded during the fire test with 325 kg dead weight positioned at 2200 mm from the wall, as shown in Fig. 1.

Fig.3 : Vulcain furnace of CSTB Champs-sur-Marne, France

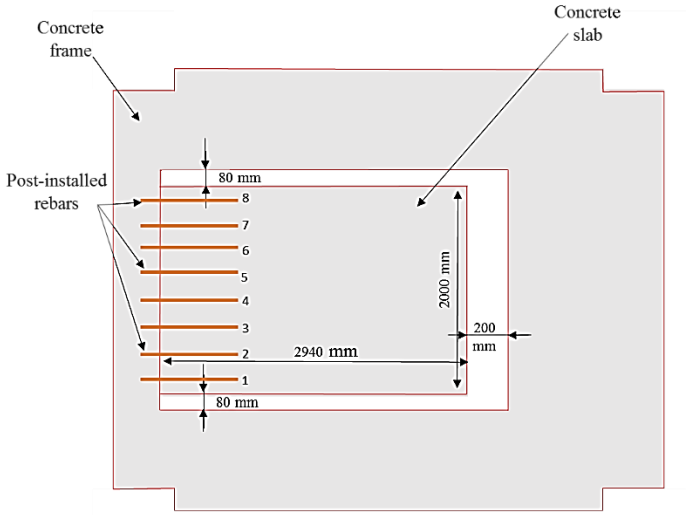

Fig. 4: Position of the slab in the concrete frame

The concrete mixture proportions are represented in Table 1. Characterization tests were carried out on cubic concrete samples (150mm x 150mm x 150mm) after 28 days of curing under ambient temperature and moisture conditions. The concrete used for the frame showed a compressive strength equal to 58.7 MPa (± 1.3 MPa) and a density equal to 2263 kg/m^3 (± 7 kg/m^3), while the concrete used for the cantilever slab presented a compressive strength equal to 22.4 MPa (± 0.3 MPa) and a density equal to 1987 kg/m^3 (± 5 MPa).

Table 1 : Mixture proportions of the concrete used for the slab and wall casting

	Unity	**Wall**	**Slab**
Cement (C)	[Kg/m^3]	280	300
Aggregate/Sand ration	[%]	107	100
Water/Cement ratio (w/c)	[%]	59	57
Superplasticizers	[% of C]	0.3	0.54
Propylene fibers	[Kg/m^3]	1.2	1.2

3.2 Design method application

3.2.1 Quantification of the applied tensile load F_{app}

Chemical post-installed rebars installed in the studied structure are subjected to tensile forces generated by vertical forces induced on one hand by the mass of the slab (5.9 kN/m), and on the other hand by the dead weight positioned at the non-exposed surface of the slab (3.2 kN at 2200 mm from the wall) (Fig. 1). Calculations showed that the total bending moment at the wall-slab interface is equal to $M_{tot} = 32.3\ kNm$. The position of the neutral axis of the slab is determined by an equilibrium of forces between the compressed area of the concrete section and the rebars. The position of the neutral axis is found equal to $Z_n = 25.5\ mm$. Hence, the pivot point position (Z_G) is determined by the position of the gravity center (G) of the triangle representing the concrete compressed area, as explained in Fig. 5. The steel strain is obtained by dividing the applied bending moment (M_{tot}) by the lever arm distance ($Z = d - Z_G$) and by the section and the elastic modulus of the steel rebars. Then, the compressive stress in the concrete section could be calculated according to *Eq. (5)*, by considering the strain compatibility between the concrete and the steel rebars. The resulting compressive force is then obtained by integrating the compressive stress over the entire thickness of the compressed zone, according to *Eq. (6)* (by assuming that the concrete deforms elastically). Finally, the total tensile force applied to the whole PIRs is therefore equal to the value of the force obtained by Eq. (6).

Nevertheless, the slab-wall connection through 8 post-installed rebars represents a statically indeterminate system. Therefore, the load distribution between the steel rebars is in reality not uniform. In order to simplify the calculations, it is supposed at this stage that the tensile force is uniformly distributed between the steel rebars. Consequently, the tensile load applied on each rebar is equal to the total tensile force divided by the number of rebars. Thus, the calculated value of the tensile force applied to each rebar is found equal to **F_{app} = 48 kN *(± 3 kN)***. The uncertainties on the applied tensile load result from the uncertainties on the position of the steel rebars in the slab, the position of the dead weight at the non-exposed surface and on the mechanical properties of steel and concrete.

$$\varepsilon_c(z) = \frac{z - z_n}{d - z_n} \quad 0 \le z \le z_n \tag{5}$$

$$F_c = \int_0^z \varepsilon_c(z).E_c.b.dz \tag{6}$$

Where d is the position of the rebars in the slab (d = 92 mm ± 4 mm)
b is the width of the slab (b = 2000 mm)
E_s is the elastic modulus of the steel rebars (E_s = 205 GPa ± 5 GPa [29]*)*
E_c is the elastic modulus of the concrete (E_c = 30 GPa ± 2 GPa [29]*)*

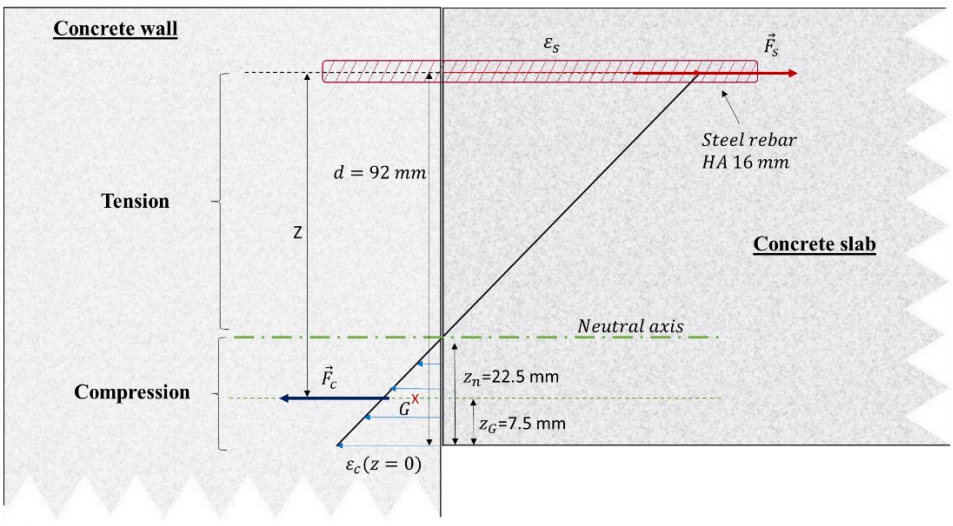

Fig. 5: Determination of the neutral axis and the pivot position in the concrete slab cross section

3.2.2 Calculation of temperature profiles (θ(x,t))

The calculation of the temperature propagation in the concrete section is carried out using a 2D finite element analysis. The studied geometry is composed of the slab section and of the entire thickness of the wall, in order to take into account the impact of the wall geometry on the temperature propagation. The mesh is created using quadrilateral elements with 4 nodes. The element size is set equal to 5 mm. The initial temperature of the entire structure before starting calculations is set equal to 20°C. The structure is then heated on the lateral surface of the wall and on the lower surface of the slab (Fig. 7) by applying convective and radiative thermal flux in accordance with the Eurocode 2 part 1-2. The gas temperature follows the ISO 834-1 time-temperature curve. The ISO 834-1 curve [36] is a conventional time-temperature curve, described by *Eq. (7)*, which reproduces the temperature increase in a structure in fire situation. The consistency of thermal calculations is checked by verifying the propagation of isotherms parallel to the exposed surface of the slab, at the furthest area from the wall/slab interface. The influence of the resin and the steel rebars on the thermal propagation is not considered in this model. The heat exchange coefficients and the thermal properties of the concrete used in thermal calculations are those provided by the Eurocode 2 part 1-2 [36] (Fig. 6) (Table 2). The thermo-physical properties of the concrete used in calculations correspond to a concrete with 1.5% moisture content.

Thermal calculations allowed obtaining the thermal distribution at the PIRs position at different times of fire exposure (Fig. 7). The thermal profiles highlights the presence of a thermal gradient along the PIRs. Indeed, the beginning of the PIRs exhibits the highest temperatures, with a high temperature increase rate, while temperatures at the bottom of the PIRs are much lower with a slower increase rate. The thermal gradient between the two ends of the PIRs increases continuously during the fire exposure.

$$\theta(t) = 20 + 345 \log_{10}(8t+1) \quad (7)$$

Where θ is the gas temperature [°C]
t is the fire exposure time [min]

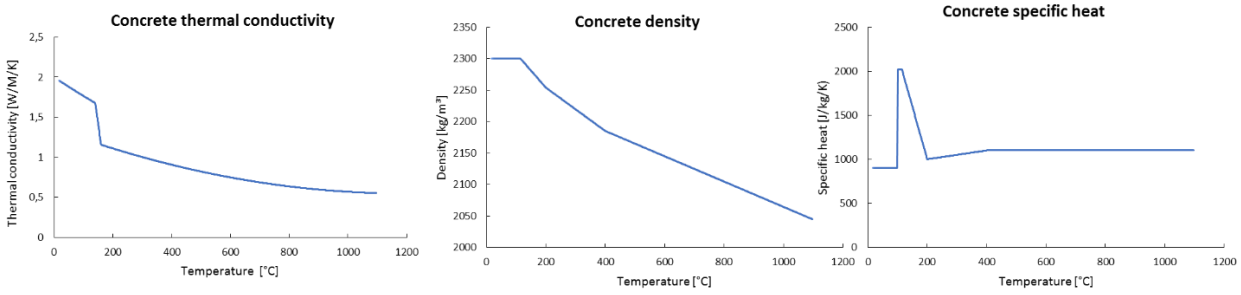

Fig. 6: Concrete thermal conductivity, density and specific heat variation under heat effect

Table 2: Heat exchange coefficients for concrete surfaces exposed and non-exposed to fire

	Convective exchange coefficient (h)	Emissivity of the concrete (ε)	Stephan-Boltzmann constant (σ)
Exposed surface	25 W/m²/K	0.7	5.67×10^{-8} W/m²/K
Non-exposed surface	4 W/m²/K	0.7	

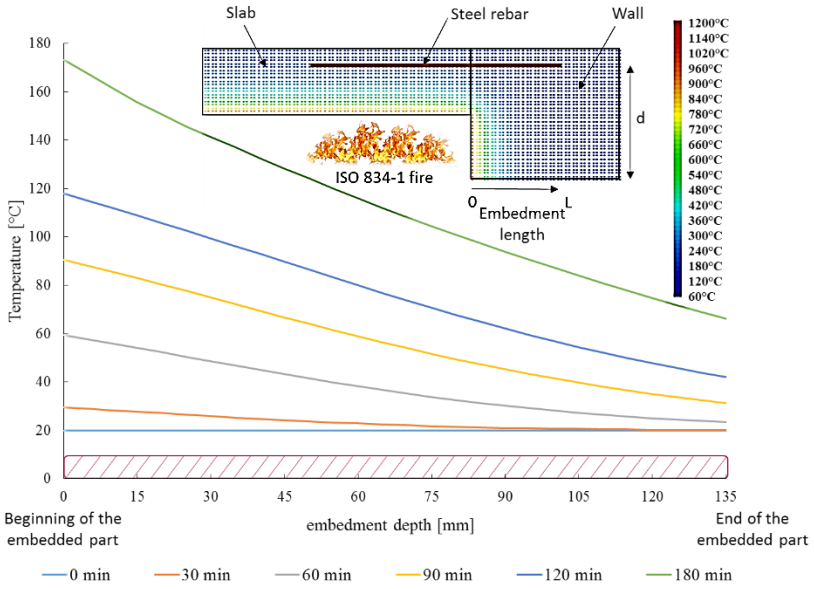

Fig. 7: Thermal distribution along the PIR at different moments of ISO fire exposure obtained by F.E. analysis

3.2.3 Bond strength – Temperature relationship ($\tau_{max}(\theta)$)

The relationship between the bond strength and temperature is obtained experimentally through pull-out tests performed by applying a constant bond stress in the adhesive joint. The description of the test procedure and the main results are presented in a previous paper [23]. The tests are performed on steel rebars bonded into concrete cylinders (160 mm diameter and 250 mm height) using the same epoxy resin than that will be used in the full-scale fire test. Steel rebars are mechanically loaded by applying a constant tensile force using a hydraulic jack. The generated shear stress in the bond joint is calculated following *Eq. (8)* by assuming a uniform stress distribution along the PIR. The applied bond stress is comprised between 3 MPa and 27 MPa. Once the constant load is applied, the concrete cylinders are heated using an electrical heating device until the total extraction of the rebars. The average temperature at failure is measured by two thermocouples positioned at the end and at 10 mm from the top surface of the bond. Therefore, for each pull-out test, a failure temperature is associated to a given bond resistance. Pull-out test results are shown in Fig. 8. The bond resistance decay at elevated temperatures is mainly caused by a set of physical, chemical and mechanical phenomena such as resin glass transition. These phenomena are detailed and examined from experimental and theoretical point of view in a previous paper [23].

Eq. (9) represents the bond strength – temperature relationship. The bond resistance is assumed to be constant for temperatures below 27°C. The decay in the bond resistance under heating effect is described by an exponential law, which represents a good accuracy with experimental results (R=0.998). Above 115°C, the bond resistance is considered equal to zero.

$$\tau_{max} = \frac{F}{\pi . d . L} \tag{8}$$

Where F is the tensile load applied on the steel rebar [N]
d is the diameter of the steel rebar [mm]
L is the embedment length [mm]
τ_{max} is the bond strength [MPa]

$$\tau_{max}(\theta) = \begin{cases} 27\ \text{MPa} & \theta \leq 31°C \\ 62.367 \exp(-0.027\,\theta) & 31°C < \theta \leq 115°C \\ 0 & \theta > 115°C \end{cases} \tag{9}$$

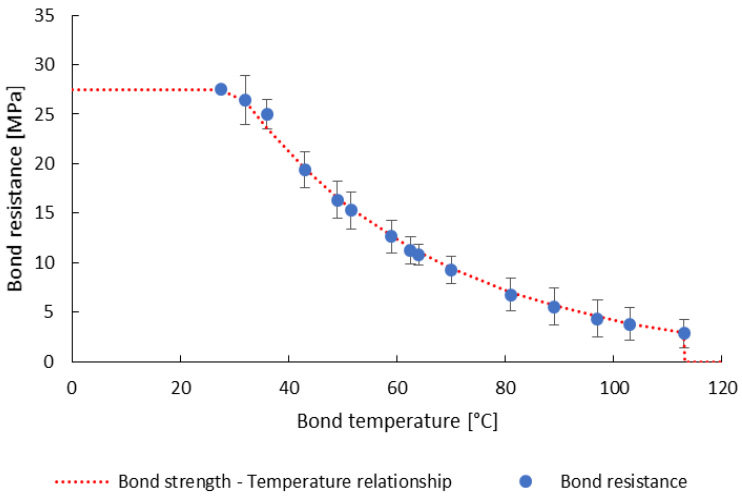

Fig. 8: Bond strength - Temperature relationship determined by means of pull-out tests at constant load [23]

3.2.4 Bearing capacity evolution and time of collapse prediction

Using calculated thermal profiles (Fig. 7) and the bond strength-temperature relationship (Fig. 8), a bond resistance value is assigned to each element of the PIR at different times of fire exposure, according to its temperature. The predicted evolution of the bond resistance profile at different moments of fire exposure is shown in Fig. 9. Results show a constant bond resistance at the beginning of the fire test (t = 0 min) equal to 27 MPa, when the entire bond is at 20°C. As the temperature increases along the bond during heating, the bond resistance decreases progressively. The decay in the bond resistance is more significant at the beginning of the PIR than that at its end. This can be attributed to the important thermal gradient present along the embedded part of the steel rebars (paragraph 3.2.2). Therefore, the most resistant parts of the PIR are located at its end, where temperatures are relatively low. Thus, the thermal gradient leads to a new bond stress distribution along the PIR with a stress concentration in the coolest zones. By heating the slab, the temperature continues to increase along the PIR and therefore the bond resistance decreases. Calculations predict that after 180 minutes of ISO fire exposure, only 75 mm of the total bond length would resist to fire.

It is then possible to calculate the evolution of the load bearing capacity of the PIR, as described in paragraph 2, by the use of data from Fig. 9 and *Eq. (4)*. Fig. 10 represents the evolution of the PIR load bearing capacity during the ISO fire exposure with margins of uncertainties resulting from the bond strength – temperature relationship (Fig. 8). The applied tensile load is represented in Fig. 10 by the horizontal lines, including the corresponding uncertainties (F_{min} and F_{max}).

The time of the slab collapse is determined by the intersection between the bond resistance curves and the applied load curves. The first intersection point corresponds to the safest time of collapse. It is obtained from the intersection between the bond resistance evolution curve indicating the lowest resistance values with the applied load curve indicating the highest values of tensile force (F_{max}). While, the last intersection point is the least safe. It corresponds to the intersection between the bond resistance evolution curve indicating the highest bond resistance values with the applied load curve corresponding to the lowest tensile load values (F_{min}). Therefore, obtained results predict a potential collapse of the slab between **114 min** and **136 min** of ISO 834-1 fire exposure for 48 kN (± 3 kN) tensile force applied to each PIR.

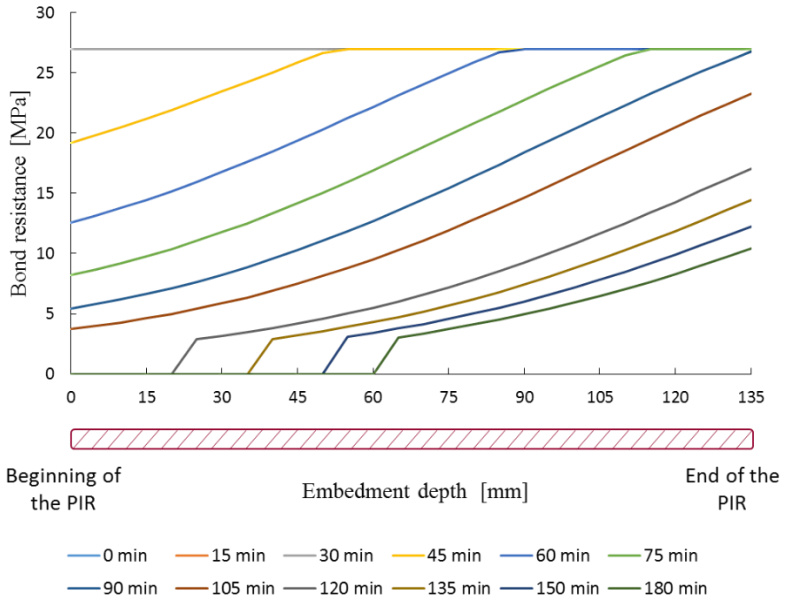

Fig. 9: Evolution of the PIR bond resistance during an ISO fire exposure

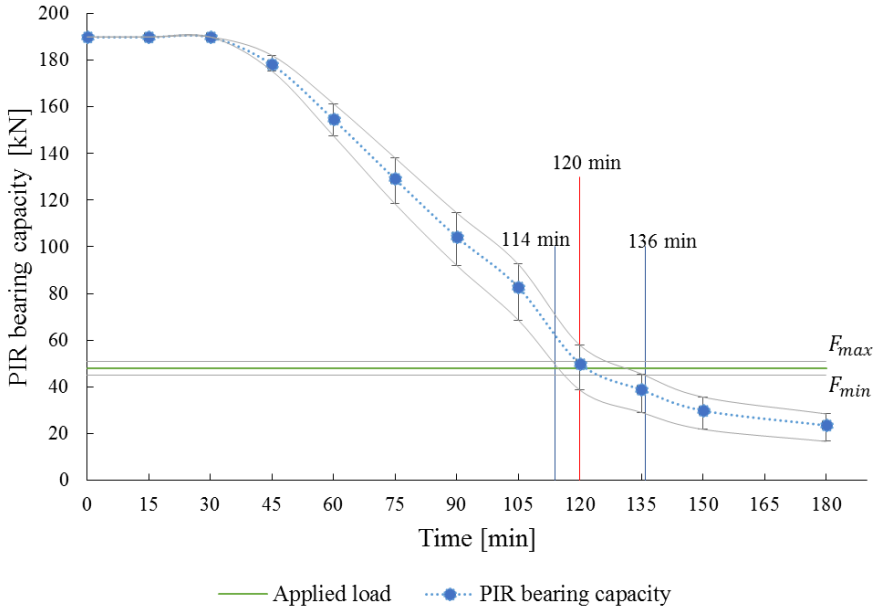

Fig. 10: Evolution of the load bearing capacity of the PIR during ISO fire exposure

3.3 Metrology

3.3.1 Temperature measurements

In order to study the temperature increase during the fire test, rows of thermocouples are installed at different positions in the test specimen (Fig. 1). 5 rows of thermocouples are introduced horizontally into the wall (portion of the concrete frame in which the chemical post-installed rebars are embedded) at the same height as the PIRs, and positioned respectively at 111mm, 555mm, 1000mm, 1450mm and 1889mm from the lateral side of the slab . Each row is composed of 5 thermocouples positioned respectively at 10mm, 20mm, 30mm, 100mm and 150mm depth. These thermocouples measure the temperature increase along the PIRs during the fire test. In addition, 3 rows of thermocouples are introduced vertically at the mid-width into the slab, at 500mm, 1500mm and 2440mm respectively from the wall. Each row is composed of 5 thermocouples positioned respectively at 10mm, 20mm, 30mm, 70mm and 100mm depth from the fire exposed surface of the slab. These thermocouples

measure the temperature increase inside the slab during the fire exposure. Finally, the gas temperature inside the oven is controlled by 6 pyrometer plates located below the test specimen.

3.3.2 Displacement measurements

The measurement of the vertical displacement of the slab during the fire test is carried out using three wire displacement sensors attached to the slab at 2600mm from the wall and at 500 mm, 1000 mm and 1500 mm from the lateral side of the slab (Fig. 1). These displacement sensors are attached to a metallic beam positioned above the test specimen, allowing the measurement of the relative displacement between the slab and the concrete frame (Fig. 11).

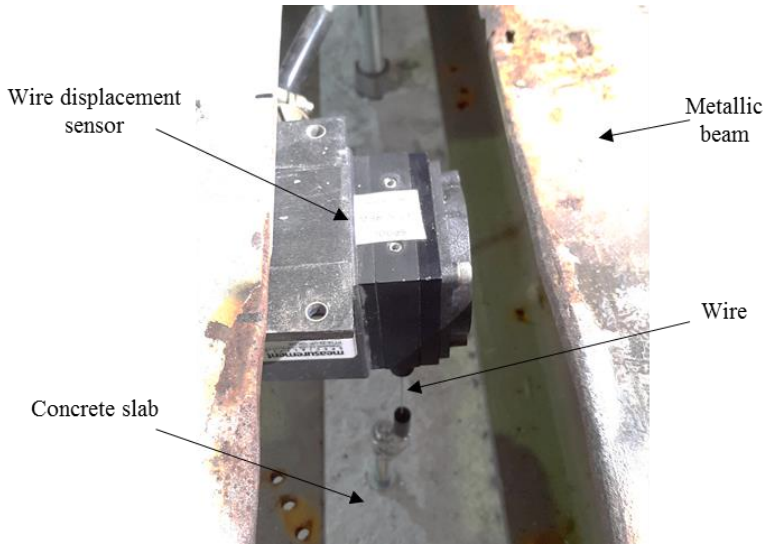

Fig. 11: Wire displacement sensor installed on the concrete slab

In addition to displacement sensors, a stereo digital images correlation system (DIC) is positioned above the test specimen in order to measure the displacement fields during the fire test (Fig. 12). Besides displacement measuring, the digital images correlation system will help in the analysis of the curvature of the slab under the temperature effect during the fire test.

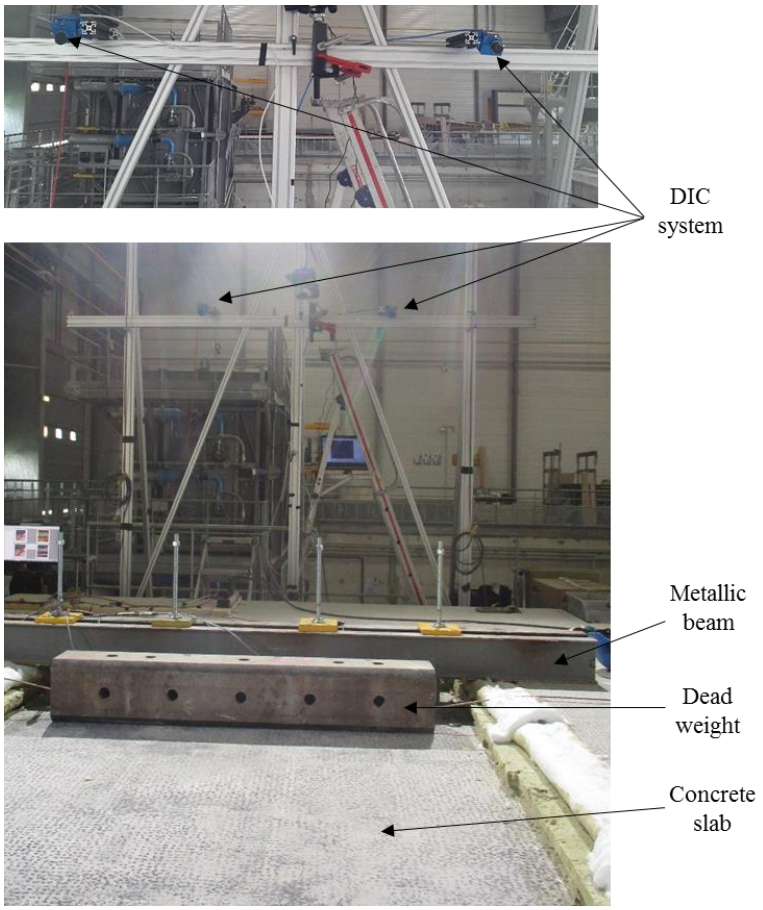

Fig. 12: Digital Image Correlation System installed above the test specimen

3.3.3. Slab rotation measurements

Two inclinometers are installed at the non-exposed surface of the slab, at 2400 mm from the wall and respectively at 500 mm and 1500 mm from one lateral side of the slab (Fig. 13). These two inclinometers allow the measurement and the analysis of the slab rotation in directions X and Y under the heat effect during the fire test.

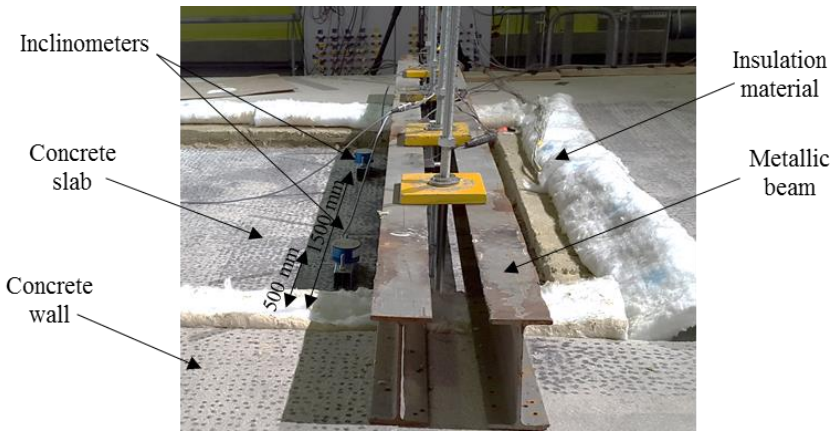

Fig. 13: Inclinometers installed at the non-exposed surface of the concrete slab

3.3.4 Wall/slab interface displacement

9 Invar bars are installed horizontally in the test specimen in order to measure the slip of the PIRs during the fire test. In fact, the Invar is a nickel-iron alloy, known for its very low thermal expansion coefficient [37] and therefore, expands very little when it is heated. Consequently, the sliding of the Invar bars during the fire test corresponds to the relative displacement between the slab and the

concrete wall. Indeed, these Invar bars are on one hand welded to the slab reinforcements and in the other hand cross the concrete section of the wall through holes drilled with a diameter equal 1.5 times the diameter of the bars, in order to ensure their free sliding during the fire test and to prevent their friction with the concrete.

The Invar bars are divided into 3 rows positioned respectively at 555 mm, 1000mm and 1455 mm from one lateral side of the slab (Fig. 14). Each row is composed of 3 Invar bars, positioned at 25 mm, 75 mm and 125 mm height respectively from the surface of the slab directly exposed to fire. Behind each of these Invar bars, an LVDT sensor (Linear Variable Differential Transformer sensor) is installed to measure the displacement of the bars relatively to the surface of the wall during the test. Therefore, these bars will help in determining both the average amount of the PIRs slip and the slab rotation during the fire test.

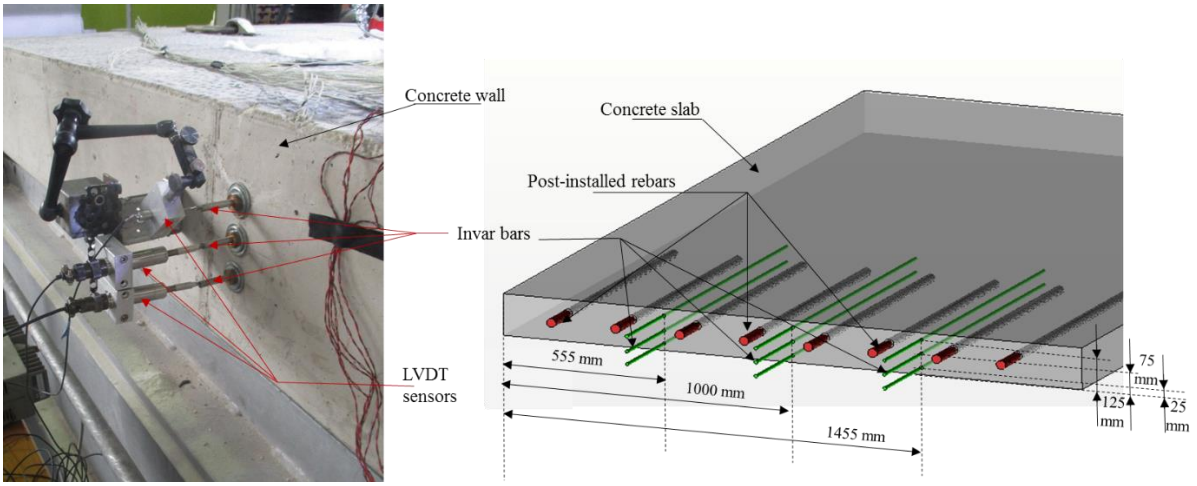

Fig. 14: Positions of the Invar bars and LVDT sensors in the test specimen

4. Results and discussion

4.1 Experimental observations

Several verification tests of the metrology and the acquisition systems were carried out before performing the full-scale fire test. The purpose of these tests was to verify the proper functioning of the metrology in order to avoid any unforeseen that might occur during the fire test. The full-scale fire test was performed 123 days after the slab concrete casting and 196 days after the concrete frame casting. The gap between the slab and the concrete frame was filled with thermal insulation material (Fig. 13) in order to confine heat. The fire exposed surface of the test specimen was continuously observed during the test with an endoscopic camera. During the heating, no concrete spalling was noticed. The slab collapsed after **117 minutes** of ISO fire exposure, when the temperature inside the gas furnace was of 1045°C, i.e. in the time interval predicted by the design method. The gas burners were turned off after the slab collapse. A loss of concrete occurred during the cooling along the slab length, on the lower surface up to the reinforcement. The slab collapse was caused by the slip of the bonded rebars. No concrete cone failure was noticed. The failure mode is investigated further in this paper.

4.2 Thermal distribution analysis

Fig. 15 represents the evolution of calculated and the average measured temperatures in the wall, at the PIRs position. The dotted lines represent the evolution of the calculated temperatures and the full lines represent the evolution of the average measured temperatures. The analysis of measured thermal profiles, recorded by the thermocouples installed horizontally in the concrete wall, shows that the slab heating had generated a thermal gradient along the PIRs. Indeed, the beginning of the bonded rebars exhibited the highest temperatures, while the end of the PIRs showed the lowest ones. Despite the fact that measurements of the gas temperature inside the furnace show that the heat was uniformly

distributed on the whole test specimen (Fig. 17), a temperature difference between the rebars was noticed. The maximum temperature difference was recorded between the rebar N°1 and N°8 (Fig. 4), at the beginning of the bond position. The maximum temperature value was reached at the beginning of the first PIR and was equal to 97°C. The temperature difference between rebars N°1 and N°8 was around 20°C. However, temperatures at the end of the bond were close ($\Delta\theta_{max}$ = 4°C). This temperature difference can be attributed to the fact that temperature measurement is very sensitive to the position of thermocouples. Indeed, the uncertainty on the position of a thermocouple can be estimated at ± 2 mm. Due to the high thermal gradient at the beginning of the bond, the uncertainty on the measured temperature is about ± 13°C at 10 mm depth, while the uncertainty on the measured temperature is about ± 2°C at 100 mm depth.

Fig. 15 shows that temperatures measured along the PIRs had not exceeded 100°C over the entire fire test duration. Indeed, the temperature had increased continuously during the first 90 minutes of fire exposure and then, a plateau was formed at the first 30 mm depth of the bond. This plateau can be the result of the water vaporization at the beginning of the bond and its accumulation in the coolest neighboring zones, which slowed down the temperature increase by consuming the thermal energy supplied by heat.

The superposition of measured and calculated temperatures reveals that calculated temperatures are close to measured temperatures, with a maximum difference around 30°C. The slight difference between measured and calculated thermal profiles can be explained on one hand by the use of theoretical values of emissivity (ε) and convection factor (h) in thermal calculations, provided by the Eurocode [36]. Indeed, values provided by the Eurocode are generally multiplied by a safety factor, and lead therefore to an overestimation of the thermal propagation in the concrete section [26]. On the other hand, the temperature difference can be attributed to the non-consideration of the steel rebars contribution when measuring temperatures with thermocouples. In fact, the bonded rebars were extended into the concrete slab. The heating of slab had generated a temperature increase in the rebars which transferred the heat to the end of the bond. However, thermocouples installed in the concrete wall were fixed to a steel rod which was not extended into the slab. Therefore, thermocouples measured only the temperature increase in the concrete section of the wall and did not consider the contribution of the steel rebars in the heat transfer. Consequently, the temperature of the PIRs measured by thermocouples could be slightly underestimated.

Fig. 16 represents the evolution of calculated and the average measured temperatures in the concrete section of the slab. The dotted lines represent the evolution of the calculated temperatures and the full lines represent the evolution of the average temperatures measured by the vertical lines of thermocouples (paragraph 3.3.1). Measured temperatures highlight the presence of a plateau which takes place near 100°C, reflecting the water vaporization inside the concrete. Indeed, the vaporization of the water retained in the concrete was observed during the fire test through a water condensation at the non-exposed surface of the slab. The duration of the vaporization plateau is very short for areas close to the fire exposed surface, and increasingly long for the furthest areas.

The comparison between calculated and measured temperatures inside the slab shows that the model allows predicting correct temperature values for the first minutes of heating. However, the formation of the water vaporization plateau leads to a large gap between the calculated and measured temperatures. Indeed, calculated temperatures are considerably higher than measured temperatures when temperature exceeds 100°C. For example, at 10 mm depth inside the slab, the difference between measured and calculated temperatures is about 212°C after 100 minutes of ISO fire exposure. In fact, the temperature difference is the result of the water vaporization phenomenon which slowed down the temperature increase in the concrete section. The retarding effect of the vaporization plateau on the temperature propagation is simulated by a peak of specific heat between 100°C and 115°C (Fig. 6). However, the variation of the specific heat with temperature provided by the Eurocode do not fully reproduce the effect of the water vaporization plateau in delaying the temperature increase in the

concrete section. Hence, calculated temperature profiles are overestimated. Consequently, thermal calculations using materials thermal properties provided by the Eurocode [36] lead to a conservative thermal distribution when temperature exceeds 100°C.

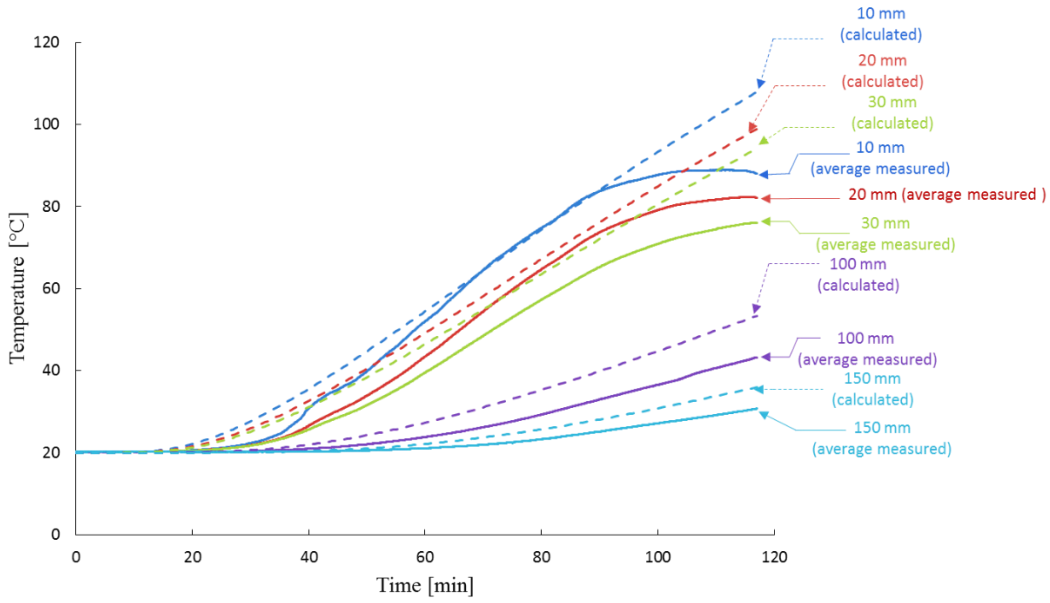

Fig. 15: Evolution of the average measured temperatures along the horizontal thermocouple lines

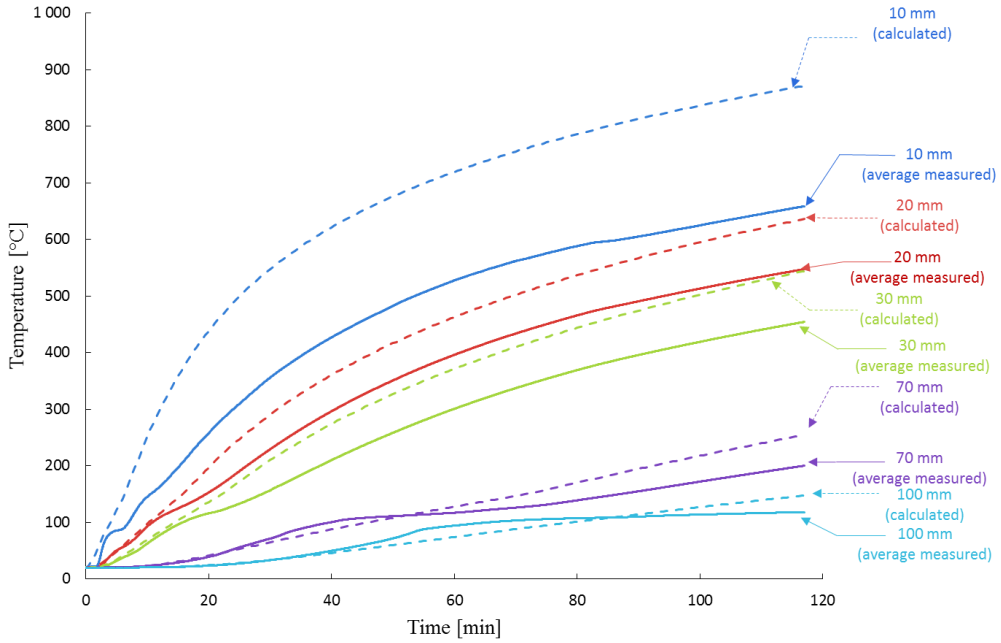

Fig. 16: Evolution of the average measured temperature along the vertical thermocouple lines

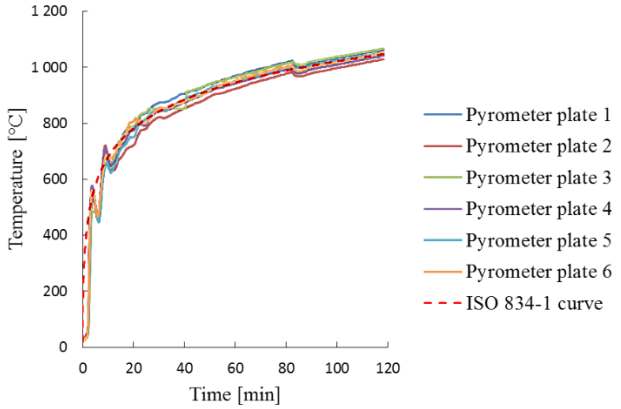

Fig. 17: Evolution of the gas temperature measured during the fire test

4.3 Slab displacement analysis

Displacements recorded by the wire displacement sensors (paragraph 3.3.2) are shown in Fig. 18. The moment of the ignition of the burners is set as the reference time in the measurement of the vertical displacement of the slab. Consequently, vertical displacements shown in Fig. 18 represent only the displacement of the slab during the fire test.

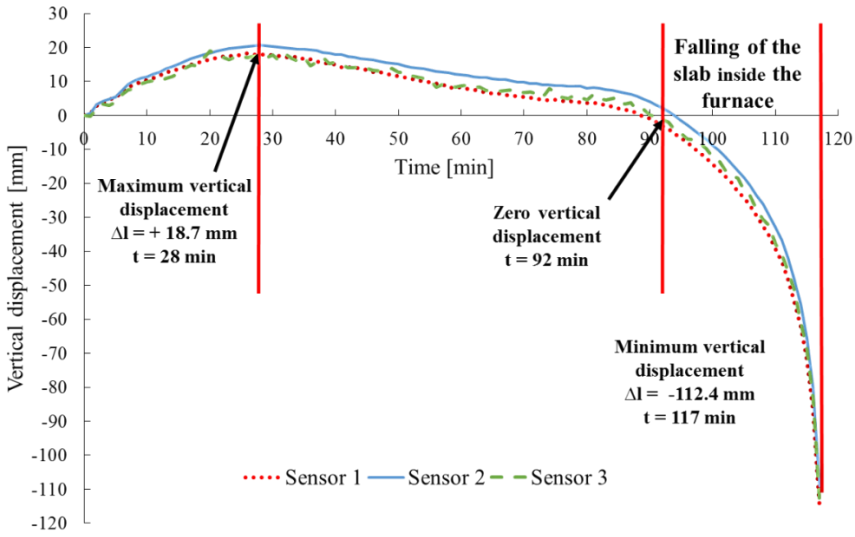

Fig. 18: Vertical displacement evolution during the fire test

The three wire displacement sensors had recorded a positive vertical displacement of the slab since the first minutes of heating. In fact, the positive vertical displacement of the slab is mainly due to a differential thermal expansion phenomenon created in the concrete section under thermal effect. Indeed, the concrete in contact with fire was rapidly heated and therefore expended considerably under the temperature effect. However, temperatures at the areas far from the fire exposed surface were relatively low. Consequently, a thermal gradient was created in the concrete section and generated a differential thermal expansion between the two surfaces of the slab, leading to its upward displacement.

By pursuing the heating of the slab, the temperature at the areas near to the exposed surface had continued to increase leading to their expansion. Thus, the slab had continued to rise upward until reaching a maximum value of vertical positive displacement. The maximum positive displacement value recorded during the fire test was equal to +18.7 mm, reached after 28 minutes of ISO fire 834-1 exposure ($\theta_{gas}(28\ min)$= 832°C)). The upward vertical displacement of the slab can be estimated analytically from the calculation of the thermal stress generated in the cross-section of the slab.

Analytical calculations, not shown in this paper, gave values very close to those measured during the fire test. After 28 min of heating, the positive vertical displacement started to decrease gradually and the slab started falling slowly inside the furnace. The zero value of vertical displacement was reached again after 92 minutes of heating. After that, the fall of the slab inside the furnace was continued until the collapse.

The fall of the slab inside the furnace could be attributed to the slip of the PIRs as a result of the temperature increase. Indeed, as explained in paragraph 3.2.4, the temperature increase along the PIR leads to decrease its mechanical properties and therefore causes its slip. Fig. 18 shows that starting from 109 minutes of fire exposure, the negative displacement of the slab was accelerated until the total failure of the PIRs and the collapse of the slab after **117 minutes** of fire exposure. The time of collapse was selected as the moment when the negative vertical displacement rate exceeded 10 mm/min. The negative vertical displacement acceleration observed at the end of the fire test can be explained by the rapid decay in the PIRs bearing capacity under the temperature effect, leading to the collapse of the slab.

Displacements recorded by the three wire displacement sensors during the fire test shows that the values measured by the sensor positioned at the mid-width of the slab (sensor 2) are slightly higher than those measured by the two lateral sensors (sensor 1 and 3), which indicate sensitively identical values. This assumes that under the heat effect, the concrete slab was curved symmetrically to an axis passing through its mid-width plan. This assumption is confirmed by the results obtained from the digital images correlation system (DIC) as shown in Fig. 19. In fact, DIC results shows the creation of displacement fields concentrated in the center of the slab during fire exposure, reflecting the bending of the slab symmetrically to its center.

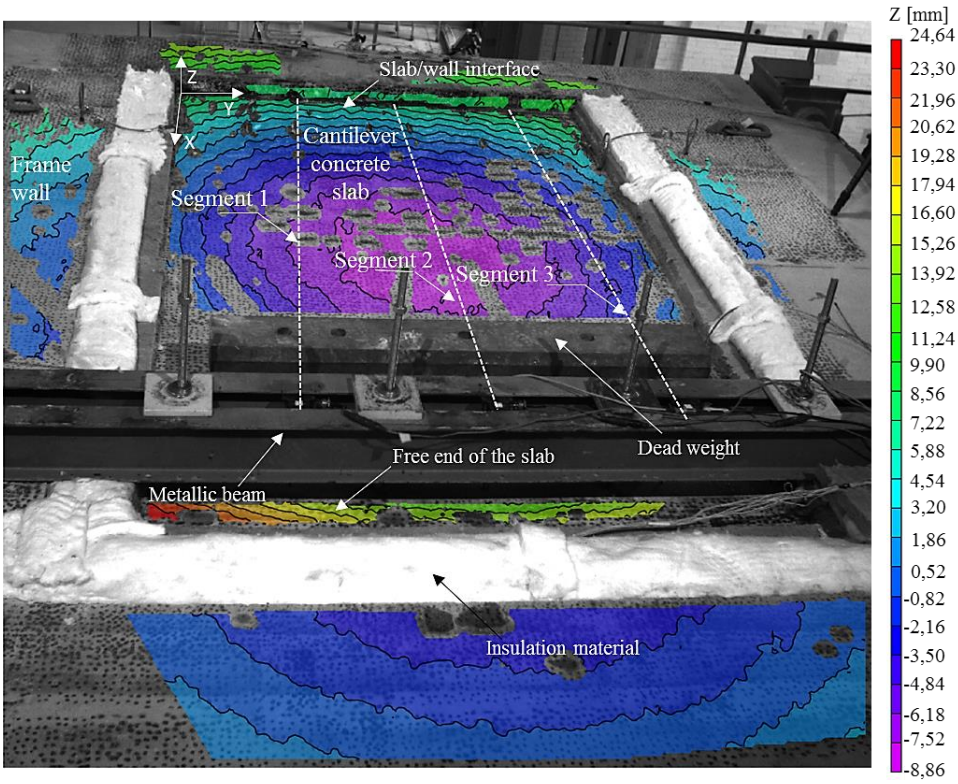

Fig. 19: Fields of vertical displacement recorded by DIC during the fire test

Using data collected from the DIC system, it is possible to plot the evolution of the slab curvature during the fire test. The slab curvature is reconstituted by plotting the evolution of the vertical displacement of three straight lines passing from the three wire displacement sensors position, designated by segment 1, 2 and 3 (Fig. 19). The displacement measurements provided by the DIC

system are identical to those measured by the wire sensors. As observed above, the measured vertical displacements in the mid-width of the slab are greater than displacements recorded at the lateral sides due to the symmetrical curvature of the slab in its center under the thermal effect.

The evolution of the slab curvature presented in Fig. 20 shows that the maximum vertical displacement was reached around 30 minutes of ISO fire exposure. After that, the slab started to fall progressively inside the furnace due to a rotation at the wall/slab interface. The rotation of the slab can be explained by the PIRs sliding under the thermal effect as explained in the previous paragraph. The curves show that the differential expansion of the slab was continued until 90 minutes of heating, highlighted by the curvature of the slab in its center. After 90 minutes of heating, a change in the shape of the slab was observed. The curvature of the slab in its center was less pronounced and the negative vertical displacement had become more important. This fact can be explained by the decay in the thermal gradient between the exposed and unexposed surface of the slab.

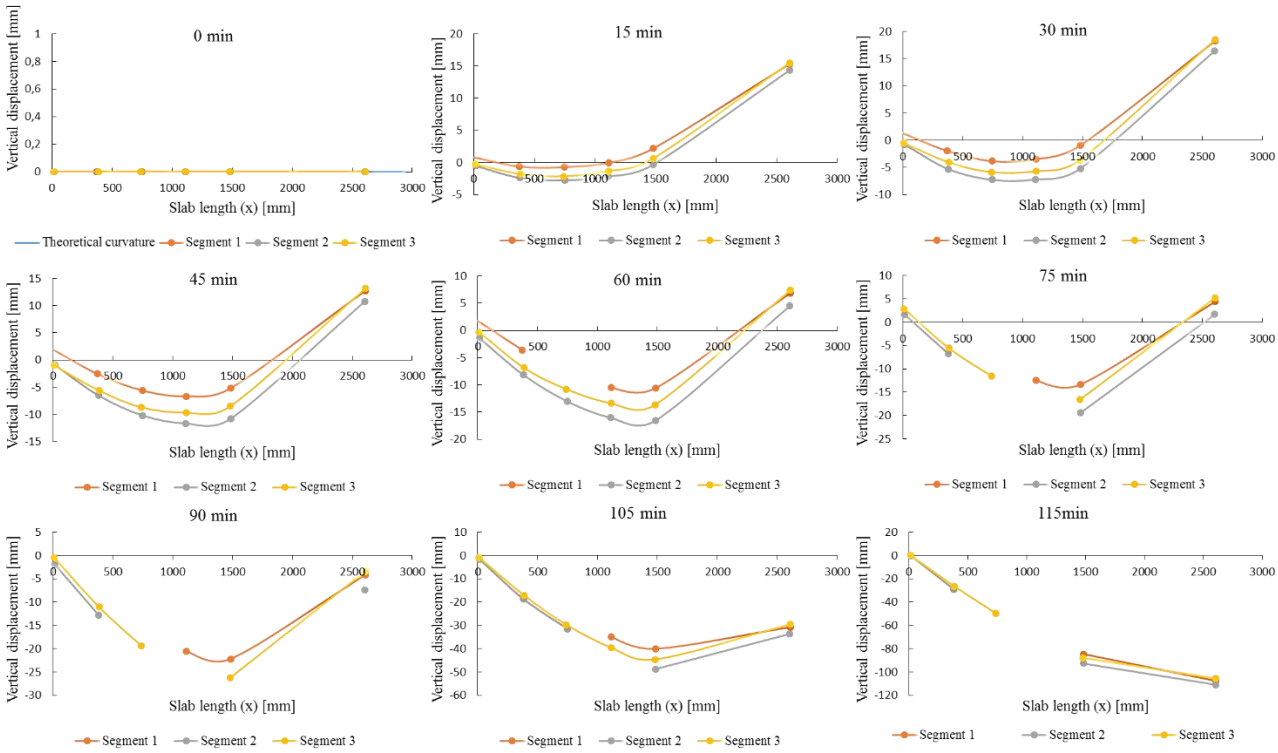

Fig. 20: Evolution of the curvature of the slab during the fire test plotted from the DIC data

4.4 Slab rotation analysis

Fig. 21 shows the slope evolution of the slab in the X and Y directions. The inclinations along the X-axis recorded by the two inclinometers were sensitively identical over the entire fire test duration (*Fig. 21 a*). Curves show a constant increase rate of the slab inclination in the X-axis direction up to 28 minutes of fire exposure. As a reminder, 28 minutes corresponds to the moment when the maximum positive vertical displacement was reached. After 28 minutes, the curvature of the slab had continued to increase but with a slower increasing rate until reaching a maximum value equal to +1.39° at 92 minutes of fire exposure. This observation confirms the fact that the differential thermal expansion of the slab was not interrupted until 92 minutes of heating. After 92 minutes, the slab started to fall inside the furnace and the inclination value in the X-axis direction started to decrease. The zero inclination value was reached for the second time at 115 minutes of fire exposure. Therefore, the recorded inclination value at the moment of the slab collapse (117 minutes) was negative. The sign change of the slab rotation following the X-axis indicates a reversal curvature of the slab and confirms the change of its shape at the last minutes of the fire test, as shown in paragraph 4.3, indicating the collapse.

Inclinations recorded along the Y-axis were almost symmetrical (*Fig. 21 b*), which confirms the curvature of the slab symmetrically to its center. Curves highlights a constant increase rate of the slab rotation in the Y direction up to 28 minutes of fire exposure. After 28 minutes, a change in the rotation increase rate is observed. Results in Fig. 21 b) indicate that the slab had continued to curve under the thermal effect with a slower rate until failure, which confirms that the differential thermal expansion of the slab in the Y-axis direction was not interrupted during the test.

The inclination analysis pointed out that the curvature of the slab under thermal effect was continued until at least the moment of the slab falling inside the furnace. Finally, the slab curvature analysis allowed to notice that the decay in the load bearing capacity of the PIRs under temperature effect had started to become critical from 92 minutes of fire exposure.

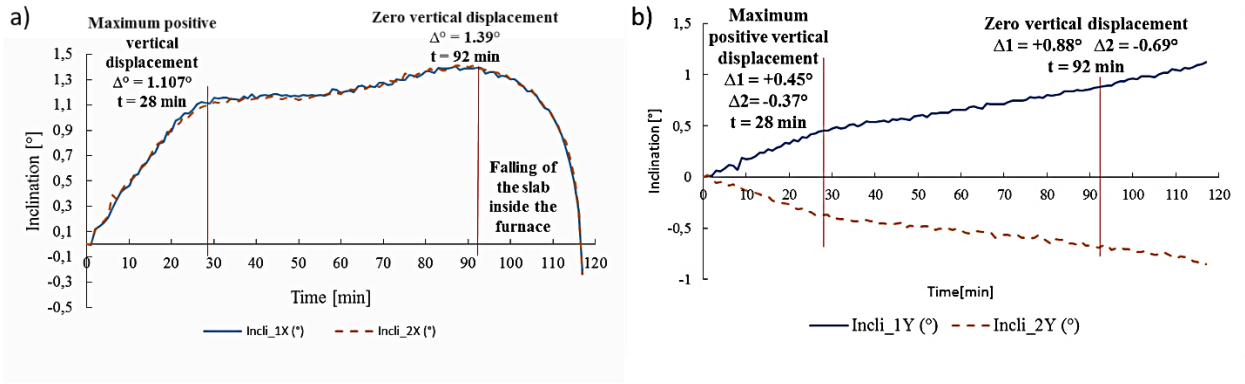

Fig. 21: Slab curvature during the fire test. a) Along the X-axis. b) Along the Y-axis

4.5 Invar bars displacement

As mentioned in paragraph 3.3.4, three rows of Invar bars were installed in the test specimen in order to measure the PIRs slip and the slab rotation during the fire test. The evolution of the PIRs slip during the fire test is presented in Fig. 22. The curve shows that during the first 5 minutes of heating, the PIRs slip was almost equal to zero. After 5 minutes of ISO fire exposure, the slip of the rebars started to increase with a constant increase rate until reaching a slip value equal to 0.7 mm at 82 minutes of heating. Starting from that moment, the rebars slip rate was accelerated following an exponential trend until the failure of the bond after **117 minutes** of fire exposure. The maximum value of the rebars slip was recorded at the moment of the slab collapse and was equal to 2.8 mm.

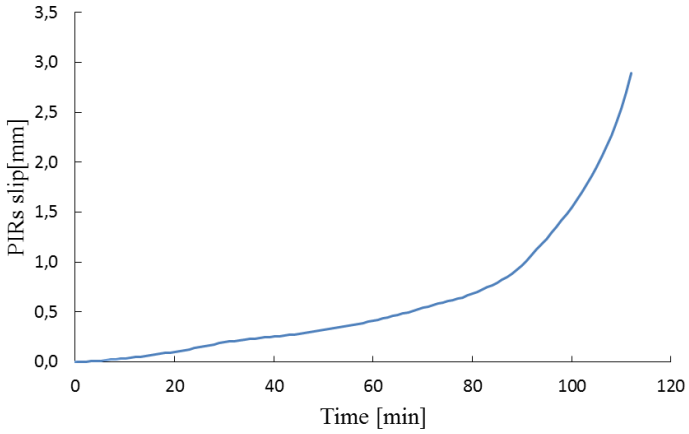

Fig. 22: Evolution of the PIRs slip during the test measured by the Invar bars

In addition to the measurement of the PIRs slip, the Invar bars were used to assess the rotation of the slab during the fire test. Fig. 23 represents the rotation of the slab during the fire test over a time interval of 15 minutes. At the beginning of the fire test, the wall/slab interface is supposed to be

perfectly vertical and the slab is in contact with the wall over its entire thickness. During the first 15 minutes of fire exposure, a small opening was observed at the wall/slab interface caused by a 0.1 mm rebars slip (Fig. 22), which could be generated by the mechanical loading of the slab. After 30 minutes of heating, the wall/slab interface seemed to not rotate but shifted by 0.1 mm. This shift can be attributed to the thermal expansion of the wall under temperature effect. Indeed, calculation showed that after 30 minutes of fire exposure, the wall could expand by 0.1 mm [26].

After 45 minutes of heating, a combination of rotation and horizontal translation was recorded. In fact, the slab horizontal translation can be explained by the temperature propagation in the section of the wall, which leads to an additional thermal expansion. However, the slab rotation can be explained by the slip of the PIRs under the temperature effect, which is the origin of the progressive fall of the slab inside the furnace, as described in paragraph 4.3. Starting from the 60th minute of heating, the slab rotation had become more important and was continuously increasing. The rotation of the slab is highlighted by the important sliding of the Invar bars indicating the PIRs slip (Fig. 22). This is also confirmed by the analysis of the slab curvature in Fig. 20, where it is shown that the decrease in the vertical displacement of the slab after 30 minutes of heating was mainly due to a rotation at the wall/slab interface.

After 75 minutes of fire exposure, a negative displacement values of the order of - 0.7 mm were recorded by the Invar bars positioned at 25 mm height in the slab section. This negative displacement values recorded in the bottom of the slab reflect the softening of the concrete at the wall/slab interface under high temperature effect (paragraph 4.3), leading consequently to the penetration of the slab into the softened portion of the wall.

Fig. 23 shows that the rotation movement at the wall/slab interface was accelerated during the last minutes of the fire test, and was the cause behind the slab collapse after **117 minutes** of ISO fire exposure. Hence, these results confirm that the slab collapse was essentially caused by the PIRs sliding due to the decay in their load bearing capacity under the temperature effect.

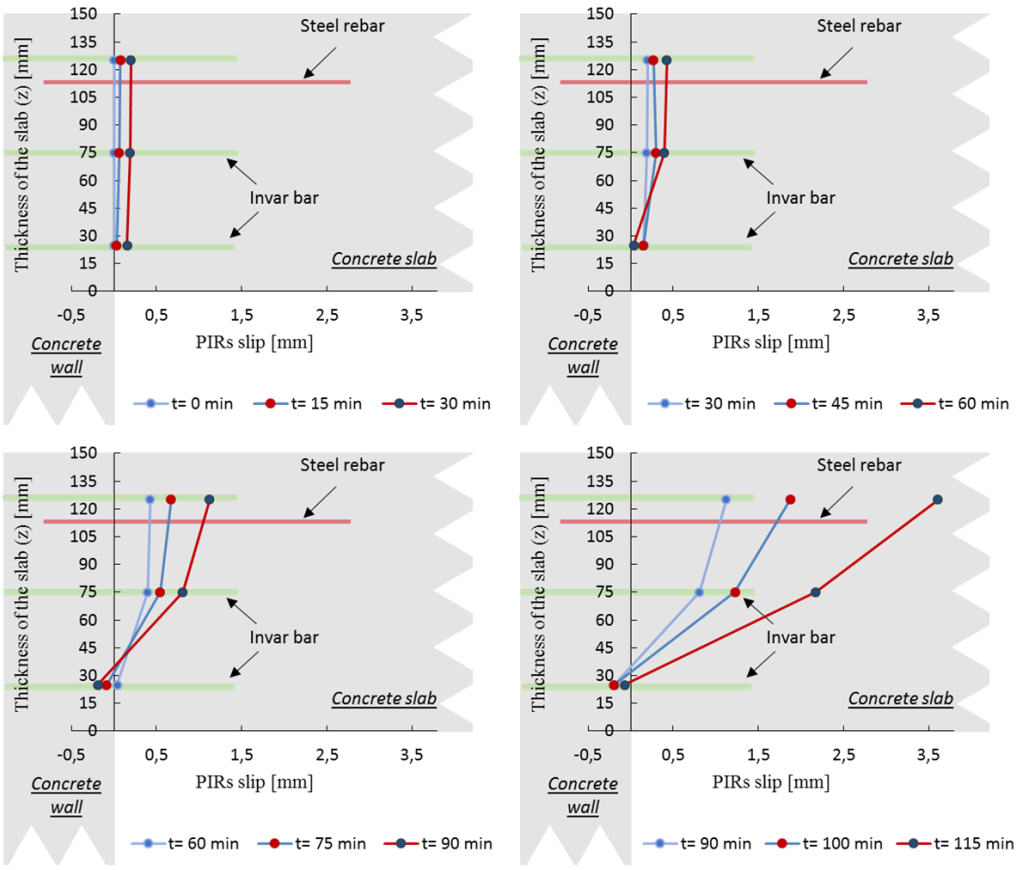

Fig. 23: Evolution of the slab rotation during the fire test measured by the Invar bars

4.6 Fracture interface analysis

The analysis of the data collected during the fire tests showed that the failure was caused by the PIRs sliding and extraction under the high temperature effect. Fig. 24 shows a section of a PIR after the fire test. The fractography analysis highlighted the presence of a mixed failure mode along the bond. A resin/concrete interface failure mode was observed at the beginning of the bond, up to the two thirds of the embedment length, while the last third of the embedded part presented a steel/resin interface failure mode. This mixed failure mode is the result of a significant thermal gradient present along the bond at the moment of failure, as confirmed by the thermal profiles recorded during the test (Fig.15). The presence of a mixed failure mode along the PIRs suggests that failure was caused by the glass transition of the epoxy resin. Indeed, the resin glass transition leads to a significant decay in the anchors load bearing capacity as mentioned in a previous paper [23]. Previous characterization tests carried out on the epoxy resin used in this fire test showed that the resin glass transition temperature was around 61°C [23]. Thermal profiles recorded along the PIRs (Fig. 15) showed that the temperature at the bond had largely exceeded 61°C, which confirms that the resin glass transition is the main cause behind the collapse of the slab.

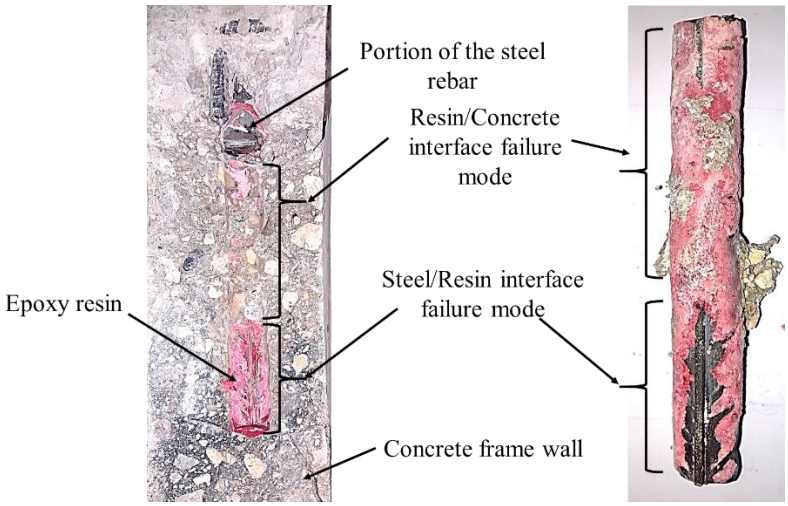

Fig. 24: Anchor's section analysis after collapse

Conclusion

This paper presents a full-scale validation test of a design method proposed for post-installed rebars in a slab/wall configuration in fire situation. The tested structure was composed of a concrete cantilever slab connected to a wall by 8 chemical PIRs, mechanically loaded by a 325 kg dead weight and thermally loaded following the ISO 834-1 time-temperature curve [36]. The time of the slab collapse predicted by the design method was comprised between 114 minutes and 136 minutes of ISO fire exposure. The prediction of the time of collapse was carried out by the determination of the PIRs bearing capacity during heating and by the quantification of the tensile force applied on each rebar. The slab collapse occurred after 117 minutes of heating. The validation test showed that the proposed design method provides a failure time close to the experimental one. Therefore, results show that the established assumptions are in good agreement with the reality.

From the analysis of the results obtained during the experimental validation test, several conclusions could be derived.

- The temperature measured along the PIRs during the fire test has not exceeded 100°C. In fact, calculated thermal profiles, using the concrete thermal properties provided by the Eurocode 2 part 1-2, allowed to correctly predict the temperature increase along the PIR, which helped in some ways to accurately estimate the time of collapse of the cantilever slab. Indeed, the superposition of thermal profiles showed that the finite element thermal model using data from the Eurocode 2 allows to precisely predict the temperatures in the concrete section as long as the temperature is below 100°C. However, above 100°C, the model is not able to predict the retarding effect of the vaporization plateau and therefore, leads to an overestimation of the temperature profiles.
- The heating of the slab during the fire test have generated a thermal gradient in the concrete section, causing a differential thermal expansion between the two surfaces of the slab, and leading to an upward vertical displacement, which should be taken into account when designing PIRs in a fire situation.
- The maximum positive vertical displacement of the slab was reached after 28 minutes of ISO fire exposure and was equal to +18.7 mm. After 28 minutes, the slab started falling inside the furnace due to the sliding of the bonded rebars, caused by the decay in their mechanical properties at high temperature.
- The analysis of displacements recorded by the DIC system during the fire test showed that the slab had curved in its center under the thermal effect. The DIC system highlighted that the

thermal curvature of the slab under the thermal effect was continued after at least 90 minutes of ISO fire exposure. After that, a change in the shape of the slab was observed, which can be the result of the concrete softening at high temperature and the attenuation of the amplitude of the thermal gradient between the two surfaces of the slab.

- The analysis of the slab rotation during the fire test showed that the PIRs sliding had become critical starting from 92 minutes of heating.
- Finally, the slab collapse was mainly caused by the slip of the chemical PIRs due to the resin glass transition.

To conclude, the analysis of the different results obtained during the fire test showed how much the design of structures in fire situation is complicated due to the intervention of several phenomena. The design method presented in this paper allowed to determine the time of collapse of PIRs directly from the evolution of the bond resistance profile and from temperature profiles, which allowed escaping all the complexities and difficulties linked to the determination of the bond stress distribution along the bond. Indeed, the determination of the bond stress distribution along PIRs in fire situation can be carried out using analytical models, and will be the subject of an upcoming paper.

Acknowledgments

The research experimental work presented in this paper was conducted at CSTB (Centre Scientifique et Technique du Bâtiment) Champs-sur-Marne, France. The authors would like to acknowledge all the technicians and executives of DSSF/MRF division, who contributed to the realization of the fire test.

References

[1] A. F. Bingöl and R. Gül, "Residual bond strength between steel bars and concrete after elevated temperatures," *Fire Safety Journal*, vol. 44, pp. 854-859, 2009.

[2] R. Eligehausen, I. Hofacker and S. Lettow, "Fastening Technique- Current Status and Future Trends," *Symposium on Connections between Steel and Concrete, 55th RILEM Annual week*, pp. 1-17, 2001.

[3] R. Cook, "Behavior of Chemically Bonded Anchors," *Journal of Structural Engineering*, vol. 119(9), pp. 2744-2762, 1993.

[4] D. Van Gemart, "Force transfer in epoxy bonded steel/concrete joints," *Int Adhes Adhes*, vol. 1(2), pp. 67-72, October 1980.

[5] N. Pinoteau, P. Pimienta, T. Guillet, P. Rivillion and S. Rémond, "Effect of heating rate on bond failure of rebars into concrete using polymer adhesives to simulate exposure to fire," *Int Adhes Adhes*, vol. 31(8), pp. 851-861, December 2011.

[6] H. Sato, K. Fujikake and S. Mindess, "Study on dynamic pullout strength of anchors based on failure modes," *13th World Conference on Earthquake Engineering*, vol. 854, August 1-6, 2004 Vancouver, B.C., Canada.

[7] T. Bickel and A. Shaikh, "Shear Strength of Adhesive Anchors," *Precast Concrete Institute Journal*, pp. 92-100, 2002.

[8] Michigan Departement Of Transportation, "Design Procedures for Concrete Anchors (Mechanical Expansion and Bonded Anchors)," Michigan Transpostation Commission, Michigan, 1998.

[9] Williams Form Engineering Corp, "Grout Bonded Concrete Anchors," 2011. [Online]. Available: http://www.williamsform.com/Concrete_Anchors/Grout_Bonded_Concrete_Anchors/grouted_concrete_anchors.html. [Accessed 28 Février 2017].

[10] P. Bardonnet, "Résines époxydes (EP) - Composants et propriétés," *Traité plastiques et composites, éditions T.I. (Techniques de l'ingénieur),* 1992.

[11] K. Benzarti, N. Houhou, M. Quiertant and S. Chataignier, "Creep behavior of cold curing epoxy adhesives: analysis and predictive approach," *Composites In Civil Engineering (CICE),* pp. Vancouver, Canada, Aug 2014.

[12] H. Spieth, J. Ozbolt, A. Eligehausen and J. Appl, "Numerical and experimental analysis of post-installed rebars spliced with cast-in-place rebars," *International Symposium on Connections between Steel and Concrete,* vol. 889, p. RILEM Publications , Sttutgart, 2001.

[13] B. Rosca and Z. Kiss, "Bond behaviour of the post-installed bundled rebars anchors with cement mortar in hardened concrete," *Buletinul Institutului Politehnic din Iasi, universtatea Tehica "Gheorghe asachi" din Iasi,* vol. LXI(LXV), pp. 117-129, 2015.

[14] A. Colak, "Parametric study of factors affecting the pull-out strength of steel rods bonded into precast concrete panels," *Int Adhes Adhes,* vol. 21(6), pp. 489-493, 2001.

[15] A. Colak, "Estimation of ultimate tension load of methylmethacrylate bonded steel rods into concrete," *Int Adhes Adhes,* vol. 27(8), pp. 653-660, December 2007.

[16] E. Nigro, A. Bilotta, G. Cefarelli, G. Manfredi and E. Cosenza, "Performance under fire situations of concrete members reinforced with FRP rods: Bond models and design nomograms," *Jornal of composites for construction,* vol. 16(4), pp. 395-406, August 2012.

[17] M. Bajer and J. Barnat, "Dependence of Ultimate Bond Stress on Bond Anchor Carrying Capacity," *Slovak Journal of Civil Engineering,* pp. 1-7, 2009.

[18] J. Meszaros and R. Eligehausen, "Einfluss der Bohrlochereiningung und vo feuchtem Beton auf das Tragvehalten von ijektions düblen (Influence of hole cleaning and of humid concrete on the load bearing behaviour of injection anchors)," Institut für Werkstoffe im Bauwesen, Universität Stuttgart , 1998.

[19] H. Spieth and R. Eligehausen, "Bewehrungsnschlüsse mit nachträglich eingemöelten bewehrungstaben (Starter bars with post installed rebars)," *Beton und Stahlebetonbau,* vol. 97(9), p. 2002, 445-459.

[20] R. Eligehausen and F. Werner, "Recent Developments and Open Problems in Fastening Technique," *2nd International Symposium on Connections between Steel and Concrete,* Stuttgart, FIB, Germany; 2007.

[21] J. Petit, V. Nassiet and Y. H.-R. B. Baziard, "Etude de la durabilité des assemblages collés," *Techniques de l'ingénieur,* p. COR160, 2005.

[22] Y. Zhang, G. Lou, K. Chen and G. Li, "Residual strength of organic anchorage adhesive for post-installed rebar at elevated temperatures and after heating," *Fire Technology Journal,* vol. 52, pp. 877-895, 2016.

[23] M.-A. Lahouar, J.-F. Caron, N. Pinoteau, G. Forêt and K. Benzarti, "Mechanical behavior changes of chemical anchors under high temperature exposure: Experimental investigation," *International journal of adhesion and adhesives,* vol. 78, pp. 200-211, 2017.

[24] J. Reis, "Effect of Temperature on the Mechanical Properties of Polymer Mortars," *Materials Research,* vol. 15(4), pp. 645-649, 2012.

[25] R. Adams, J. Coppendale, V. Mallick and H. Al-hamdan, "The effect of temperature on the strength of adhesive joints," *International Journal of Adhesion and Adhesives,* vol. 12(3), pp. 185-190, 1992.

[26] N. Pinoteau, J. Heck, R. Avnel, P. Pimienta, T. Guillet and S. Remond, "Prediction of failure of a cantilever-wall connection using post-installed rebars under thermal loading," *Engineering structures,* vol. 56, pp. 1607-1619, 2013.

[27] N. Pinoteau, Comportement des Scellements Chimiques d'Armaturesraportées pour Béton en Situation d'Incendie, Lille: Université Lille 1, 2013.

[28] U. Sorathia, R. Lyon, R. Gann and L. Gritzo, "Materials and fire threat," *Fire technology journal,* vol. 33(3), pp. 260-275, 1997.

[29] CEN, "EN 1992-1-1, Eurocode 2: Design of concrete structures - part 1-1: General rules and rules for buildings," 2004.

[30] EOTA, "ETAG 2001: European Techniques of Anchor Guideline," 2001.

[31] ACI Provisional Standards, "ACI 335.2-01, Evaluating the performance of post-installed mechanical anchors in concrete," 2001.

[32] ASTM International, "ASTM C881: Standard specification for epoxy-resin base bonding systems for concrete," 2013.

[33] C. B. I. Press, "GB 50367-2006: Design code for strengthening concrete structure," Beijing, 2006.

[34] R. Eligehausen and J. Asmus, "Expert report - Design of post-installed rebars with injection mortarFIS EM under fire exposure up to 240 min," 2008.

[35] EOTA, "EAD 330087-00-0601, Systems for post-installed rebar connections with mortar," no. EOTA 14-33-0087-06.01, July 2015.

[36] CEN, "EN 1992-1-2 Eurocode 2. Part 1-2: Design of concrete structures - General rules - Structural fire design," Bruxelles, Belgique; 2005.

[37] M. Van Schilfgaarde, A. Abrikosov, Johansson and B., "Origin of the Invar effect in iron-nickel alloys," *Nature 400,* pp. 46-49, 1999.